the FEBS Journal

# Simultaneous depletion of Atm and Mdl rebalances cytosolic Fe-S cluster assembly but not heme import into the mitochondrion of *Trypanosoma brucei*

Eva Horáková[1,*], Piya Changmai[1,2,*,†], Zdeněk Paris[1], Didier Salmon[3] and Julius Lukeš[1,2,4]

1 Biology Centre, Institute of Parasitology, Czech Academy of Sciences, České Budějovice (Budweis), Czech Republic
2 Faculty of Sciences, University of South Bohemia, České Budějovice (Budweis), Czech Republic
3 Institute of Medical Biochemistry Leopoldo de Meis, Centro de Ciências e da Saude, Federal University of Rio de Janeiro, Brazil
4 Canadian Institute for Advanced Research, Toronto, Ontario, Canada

**Keywords**
Atm; Fe-S cluster; heme; Mdl; *Trypanosoma*

**Correspondence**
J. Lukeš, Institute of Parasitology, Branišovská 31, 37005 České Budějovice, Czech Republic
Fax: +420-38-7775403
Tel: +420-38-7775416
E-mail: jula@paru.cas.cz

**Present address:**
†Life Science Research Centre, Faculty of Science, University of Ostrava, Ostrava, Czech Republic

*These authors contributed equally to this work.

(Received 5 March 2015, revised 24 July 2015, accepted 10 August 2015)

doi:10.1111/febs.13411

ABC transporter mitochondrial 1 (Atm1) and multidrug resistance-like 1 (Mdl) are mitochondrial ABC transporters. Although Atm1 was recently suggested to transport different forms of glutathione from the mitochondrion, which are used for iron-sulfur (Fe-S) cluster maturation in the cytosol, the function of Mdl remains elusive. In *Trypanosoma brucei*, we identified one homolog of each of these genes, *Tb*Atm and *Tb*Mdl, which were downregulated either separately or simultaneously using RNA interference. Individual depletion of *Tb*Atm and *Tb*Mdl led to limited growth defects. In cells downregulated for *Tb*Atm, the enzymatic activities of the Fe-S cluster proteins aconitase and fumarase significantly decreased in the cytosol but not in the mitochondrion. Downregulation of *Tb*Mdl did not cause any change in activities of the Fe-S proteins. Unexpectedly, the simultaneous downregulation of *Tb*Atm and *Tb*Mdl did not result in any growth defect, nor were the Fe-S cluster protein activities altered in either the cytosolic or mitochondrial compartments. Additionally, *Tb*Atm and *Tb*Mdl were able to partially restore the growth of the *Saccharomyces cerevisiae* Δ*atm1* and Δ*mdl2* null mutants, respectively. Because *T. brucei* completely lost the heme *b* biosynthesis pathway, this cofactor has to be obtained from the host. Based on our results, *Tb*Mdl is a candidate for mitochondrial import of heme *b*, which was markedly decreased in both *Tb*Mdl and *Tb*Atm + *Tb*Mdl knockdowns. Moreover, the levels of heme *a* were strongly decreased in the same knockdowns, suggesting that *Tb*Mdl plays a key role in heme *a* biosynthesis, thus affecting the overall heme homeostasis in *T. brucei*.

## Introduction

Every extant prokaryotic and eukaryotic cell contains iron-sulfur (Fe-S) cluster proteins, which carry one or more of these ancient inorganic cofactors. More than 100 different Fe-S proteins have been described so far, which are involved in DNA repair, oxidative phosphorylation, DNA/RNA metabolism, sensing and other cellular processes, with prominent examples including mitochondrial respiratory complexes I–III, ferredoxin,

**Abbreviations**
ABCB7, ATP-binding cassette sub-family B member 7; APM, [(*N*-acryloylamino)-phenyl] mercuric chloride; Atm1, ABC transporter mitochondrial 1; CIA, cytosolic iron-sulfur cluster assembly; ISC, iron-sulfur cluster; Mdl1, multidrug resistance-like 1; Mfrn1, mitoferrin-1; RNAi, RNA interference.

aconitase and DNA polymerases [1,2]. Even though Fe-S clusters can be spontaneously assembled *in vitro* under specific chemical conditions, their assembly *in vivo* requires complex mechanisms and regulations [3]. In eukaryotes, mitochondria inherited the iron-sulfur cluster (ISC) machinery from α-proteobacteria, while plastids are equipped with the sulfur mobilization pathway. Because they have many Fe-S proteins in the cytosol and nucleus, eukaryotes also evolved a dedicated mechanism for maturation of the cytosolic Fe-S clusters, the so-called cytosolic iron-sulfur cluster assembly (CIA) machinery for these cell compartments [1].

In the model eukaryote *Saccharomyces cerevisiae*, the mitochondrial ISC machinery is composed of the cysteine desulfurase complex Nfs-Isd11, a sulfur donor, which converts cysteine to alanine and provides sulfur to the scaffold protein Isu [2,4], whereas ferredoxin is the source of electrons for the reduction of $S^0$ to $S^{2-}$ within the Fe-S cluster [5]. Frataxin and glutathione were proposed to serve as iron donors [6,7]. Although the former protein was found to enhance the Fe-S formation in eukaryotes [8], it appears to inhibit the same reaction in prokaryotes [9]. Apart from these key components, other proteins, such as Isa1, Isa2 and Iba57, participate in transportation of the Fe-S clusters to specific mitochondrial proteins [10–12].

For maturation of their clusters, the cytosolic and nuclear Fe-S proteins of *S. cerevisiae* require the CIA machinery. Although, in mammalian cells, the cytosolic ISCU was reported to have a function in the cytosolic Fe-S proteins repair after oxidative damage and iron chelation, its role in *de novo* Fe-S synthesis is still questioned [13]. Moreover, because the cytosolic Nfs1 was unable to maintain Fe-S protein activities [14], the CIA pathway apparently depends on the mitochondrial ISC pathway, an export machinery that transports needed substrate from the mitochondria to the cytosol [3].

ABC transporter mitochondrial 1 (Atm1), a transporter located in the inner mitochondrial membrane [15], is known to be involved in Fe-S cluster [16] and molybdenum cofactor assembly in the cytosol [17]. Being exposed into the mitochondrial matrix, its C-terminus is important for coupling energy from ATP hydrolysis [18]. In *S. cerevisiae* under aerobic conditions, the lack of Atm1 causes iron accumulation in the mitochondria and an overall decrease of Fe-S clusters and heme in both the mitochondria and the cytosol, leading to oxidative damage. However, during anaerobiosis, neither Fe-S clusters, nor heme levels were affected in the yeast, which, upon depletion of Atm1, exhibited a normal level of mitochondrial iron. Furthermore, the activities of only cytosolic but not mitochondrial Fe-S proteins were impaired during anaerobiosis [19]. Because the depletion of Atm1 in *S. cerevisiae* produce markedly similar phenotypes to glutathione and sulfhydryl oxidase, it was proposed that these proteins may work together in an export activity [20,21].

The human ortholog of Atm1 is an ATP-binding cassette sub-family B member 7 (ABCB7), which interacts with the Fe-S cluster-containing ferrochelatase. This enzyme inserts ferrous ion into protoporphyrin IX in the terminal step of heme biosynthesis [22]. Mutations in ABCB7 are responsible for X-linked sideroblastic anemia with ataxia [23]. The depletion of ABCB7 in HeLa cells was reported to result in a decrease of cell proliferation, iron accumulation in mitochondria, an increase in protoporphyrin IX and a decrease in the activity of the cytosolic Fe-S proteins [23,24]. The *Arabidopsis thaliana* genome encodes three Atm1-like genes, labeled *At*ATM1 to *At*ATM3. *At*ATM3 appears to be the functional homolog of the canonical Atm1 [25] because its mutant showed a decrease of the cytosolic but not mitochondrial and plastidic Fe-S cluster protein activities [26]. In addition, the activity of catalase, a heme-containing enzyme, was unaltered [26].

Recently, the crystal structure of the free and glutathione-bound dimeric *S. cerevisiae* Atm1 revealed its membrane-bound inward-facing structure [27]. It has also been proposed that Atm1 may serve as a sulfur carrier when converted into glutathione persulfide [27]. Recently, ATM3 of *A. thaliana* and Atm1 of yeast were suggested to selectively transport glutathione polysulfide [28], whereas a closely related bacterial homologue transports glutathione and its disulfide [29].

Multi-drug resistance-like 1 (Mdl1) is an ABC transporter in the mitochondrial inner membrane of *S. cerevisiae*, which was suggested to have a role in the export of approximately 6–21-kDa peptides generated by the m-AAA protease in the mitochondrial matrix [30], although this could not be confirmed in a subsequent study [31]. The role of Mdl2, a Mdl homolog in *S. cerevisiae* which does not transport the same proteolytic breakdown products as Mdl1, remains to be established. Overexpression of Mdl1 in Δ*atm1* yeast cells was able to reduce iron accumulation in mitochondria, whereas the overexpression of Mdl1 in wild-type *S. cerevisiae* did not affect the level of organellar iron [32]. ABCB10, the mammalian homolog of Mdl, was shown to interact with mitochondrial iron importer mitoferrin-1 (Mfrn1) [33], and this complex was found to transiently bind ferrochelatase [34]. The former protein not only enhanced the stability of

Mfrn1, but also potentiated mitochondrial iron import. Recently, it was proposed that ABCB10 may have a specific role in heme *b* biosynthesis [35]. There are three biologically important forms of heme (types *a*, *b* and *c*) that differ by modifications in the porphyrin ring. Most eukaryotes are able to synthesize heme *b* from δ-aminolevulinic acid through seven universally conserved enzymatic steps [36]. Heme *b*, also called protoheme, is the most common type and represents the prerequisite for the formation of all the other hemes [37].

By contrast to a typical eukaryote, trypanosomes and related flagellates belong to a small group of organisms that do not synthesize heme *de novo* and totally rely on external heme [38]. Upon acquisition, heme is incorporated into hemoproteins, mainly the cytochromes of electron transport chain. Respiratory complex IV is the only protein complex that for its activity requires heme *a*, which is synthesized from heme *b* by two enzymatic steps [39]. We showed previously that ferredoxin, one of the key components of the Fe-S cluster pathway in *T. brucei*, is also involved in heme *a* synthesis [40], bridging these two iron-dependent cellular processes.

In the present study, we investigated the function of *T. brucei* homologues of Atm1 (*Tb*Atm) and Mdl (*Tb*Mdl) in the procyclic stage of this model protist. RNA interference (RNAi)-mediated depletion of either *Tb*Atm or *Tb*Mdl led to a moderate growth defect, yet, unexpectedly, in the case of a *Tb*Atm + *Tb*Mdl RNAi double knockdown, the growth remained unaltered. The depletion of *Tb*Atm resulted in reduced activities of cytosolic but not mitochondrial Fe-S dependent enzymatic activities and tRNA thiolation, whereas this phenotype was absent in cells downregulated for either *Tb*Mdl or *Tb*Atm + *Tb*Mdl. Moreover, both these RNAi knockdowns showed a marked decrease in mitochondrial heme content, indicating the concerted action of these two transporters.

## Results

### Identification of *Tb*Atm and *Tb*Mdl

Using the *S. cerevisiae ATM1* gene as a query against the TriTrypDB (http://www.tritrypdb.org), we identified a single homolog in *T. brucei* (Tb927.11.16930) and named it *Tb*Atm. The *Tb*Atm gene codes for a protein with calculated molecular weight 79.10 kDa. MITOPROTII (https://ihg.gsf.de/ihg/mitoprot.html) predicted its mitochondrial localization with a 0.991 probability, with the cleavage site at position 54. *Tb*Atm shares 38%, 42% and 43% amino acid sequence identity with yeast Atm1, human ABCB7 and *A. thaliana* ATM3 homologs, respectively. The gene contains conserved ABC transporter transmembrane and ATPase regions. All the heterotrophs including kinetoplastid flagellates have a single copy, whereas the photosynthetic eukaryotes usually possess at least two homologues (Fig. 1A). The internal branching of the phylogeny lacks resolution; however, the kinetoplastid sequences form a strongly supported clade at the very base of the Atm1 clade (Fig. 1A).

The same strategy was applied for Mdl, resulting in the identification of a single homolog (Tb927.11.540), labelled *Tb*Mdl. The *Tb*Mdl gene encodes a protein with predicted molecular weight 76.25 kDa, contains conserved transmembrane and ATPase regions and is likely mitochondrial (MITOPROTII score of 0.9484 probability) with position 97 as the predicted cleavage site. *Tb*Mdl shares 38%, 37% and 37% sequence similarity with human ABCB10 and *S. cerevisiae* Mdl1 and Mdl2 homologs, respectively. The presence of a single Mdl gene in most eukaryotes including *T. brucei* indicates that the two paralogs found in *S. cerevisiae* resulted from a rather unique and recent duplication event. A similar situation could be seen only in green algae where the presence of two separate lineages could be explained by an ancient duplication followed by lineage sorting (Fig. 1B). The kinetoplastids branch off as a sister clade to opisthokonts at the crown part of the tree. Because the topology lacks resolution as a result of low support of the basal branches, no reliable conclusion can be made in that respect (Fig. 1B).

### Localization of *Tb*Atm

High probability predicted by MITOPROTII for mitochondrial localization of both *Tb*Atm and *Tb*Mdl is corroborated by their MS-based identification in the *T. brucei* mitochondrial proteome [41]. We succeeded in experimentally investigating the subcellular localization of the GFP-tagged version of *Tb*Atm *in situ*. Full-length *Tb*Atm was labelled at its C-terminus with a GFP-tag [42], and the transfected *T. brucei* ProAnv PS flagellates expressing the endogenously tagged gene were subjected to fluorescence microscopy. As expected, all GFP signal clearly co-localized with the mitochondrial marker tetramethylrhodamine ethyl ester (Fig. 2), confirming the predicted mitochondrial localization of *Tb*Atm. The protein is evenly distributed throughout the reticulated mitochondrion of the PS trypanosomes.

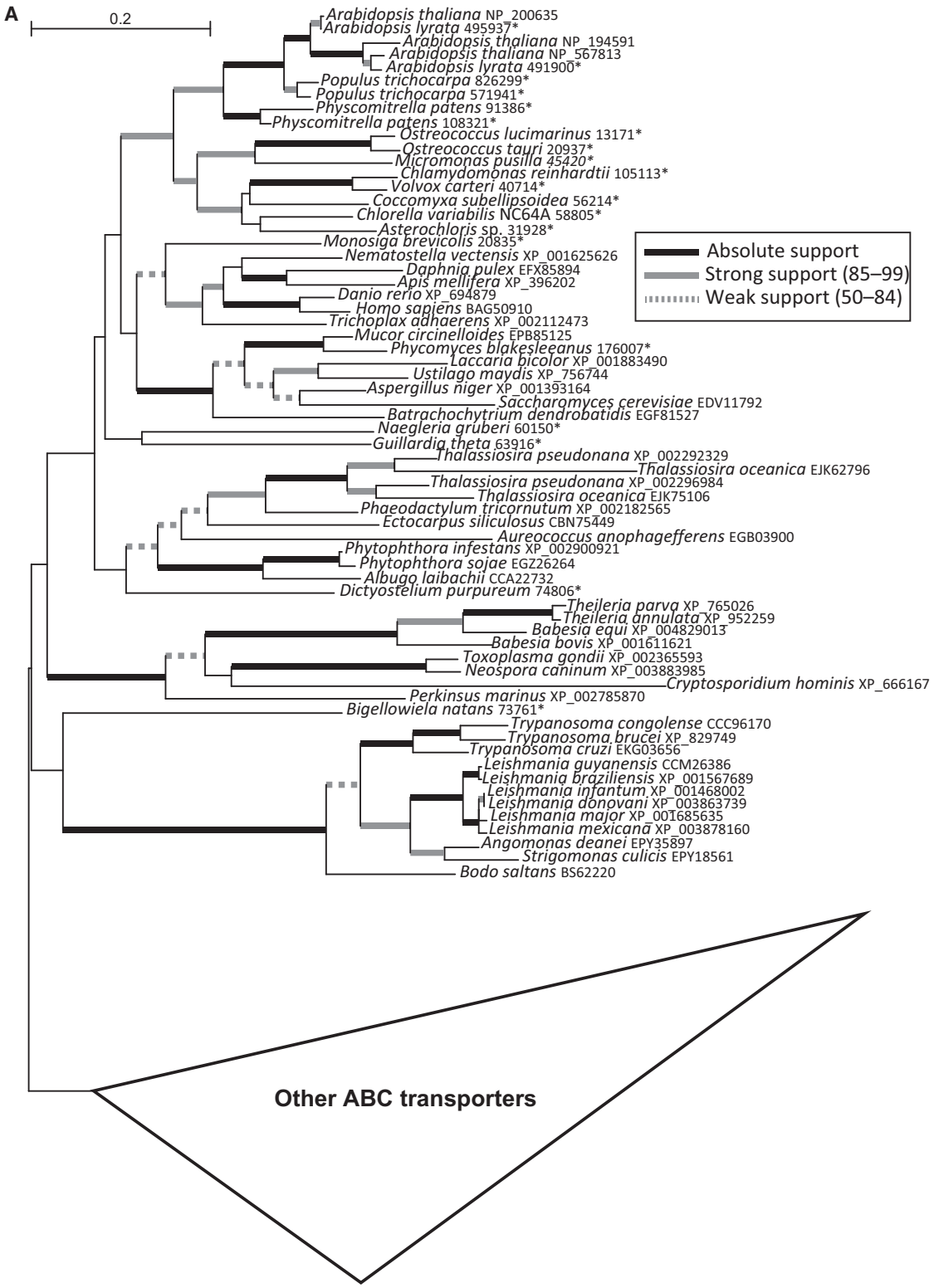


**Fig. 1.** Phylogenetic analysis of *Tb*Atm and *Tb*Mdl. Maximum likelihood phylogenetic analysis of Atm (A) and Mdl (B) inferred using RAXML and a Γ-corrected LG4X matrix (LG4X + Γ model). Branching support is expressed via nonparametric bootstrap analysis. For simplicity, the values are divided into the categories according to the strength of support (weak: 50–84, strong: 85–99 and absolute: 100). For details, see Experimental procedures. Asterisks denote sequences retrieved from JGI database.

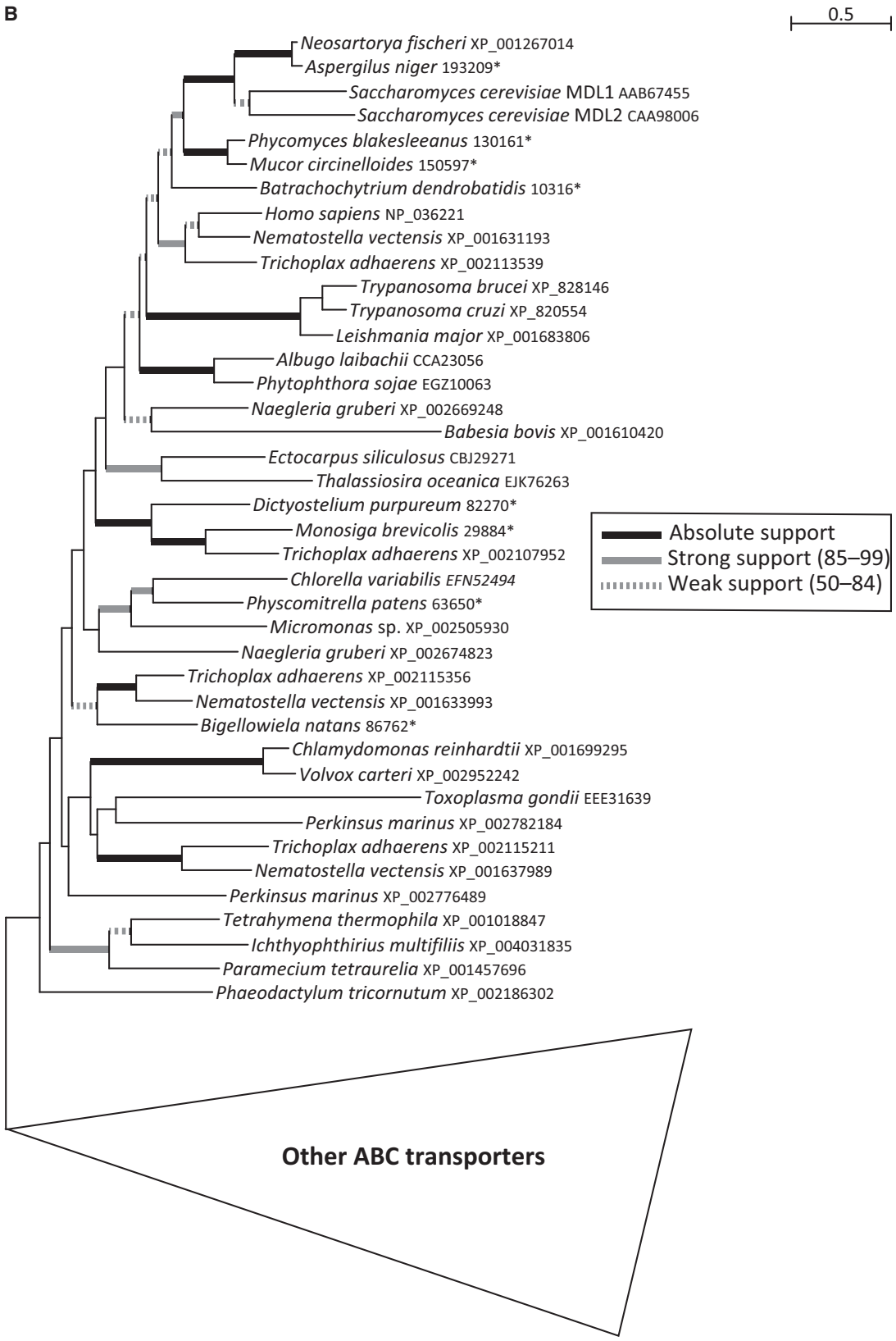


**Fig. 1.** (continued)

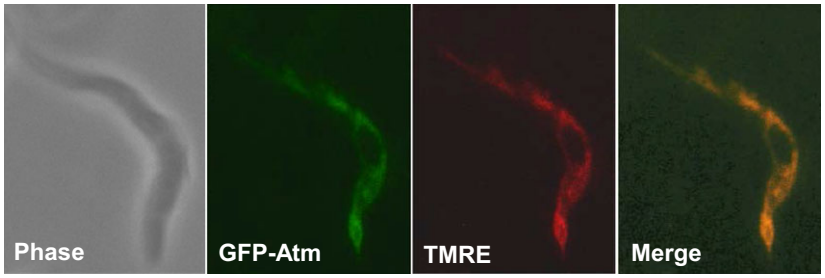


**Fig. 2.** *Tb*Atm is localized in the mitochondrion. Fluorescence microscopy of wild-type PS trypanosomes expressing *Tb*Atm GFP-tagged protein. Phase shows a picture from Nomarski contrast microscopy; tetramethylrhodamine ethyl ester visualizes the mitochondrion.

## Individual but not simultaneous depletion of *Tb*Atm and *Tb*Mdl affects viability

To investigate the functions of both ABC transporters, we used RNAi-mediated gene silencing in *T. brucei*. Fragments of *Tb*Atm and *Tb*Mdl were cloned separately into an inducible RNAi vector, and the *Tb*Atm + *Tb*Mdl double knockdown was generated by cloning both gene fragments in tandem into the same vector.

Upon RNAi induction, the *Tb*Atm-depleted cells showed slightly reduced proliferation (Fig. 3A), whereas the elimination of *Tb*Mdl resulted in a stronger growth defect (Fig. 3B). Examination of cells that lack *Tb*Atm by transmission electron microscopy did not document any mitochondrial swelling (data not shown), which is a marked difference from the phenotype observed in *T. brucei* upon the downregulation of *Tb*Erv1, another component of the Fe-S export machinery [43]. Unexpectedly, when *Tb*Atm and *Tb*Mdl were downregulated at the same time, the cell growth remained unaltered. Indeed, repeated and prolonged cultivation of the non-induced and RNAi-induced double knockdowns confirmed the absence of any growth phenotype (Fig. 3C).

The elimination of *Tb*Atm protein in both the *Tb*Atm single knockdown and the *Tb*Atm + *Tb*Mdl double knockdown flagellates was monitored by western blot analysis using specific polyclonal antibodies against the target protein. The elimination of *Tb*Atm in the single knockdown trypanosomes was efficient, with the protein being almost undetectable on day 3 post-induction, whereas the lack of any leaky transcription is exemplified by same levels of *Tb*Atm in the wild-type and non-induced cell (Fig. 3D). Western blot analysis using the same polyclonal antibody with lysates from the non-induced and RNAi-induced *Tb*Mdl single and *Tb*Atm + *Tb*Mdl double knockdowns confirmed an unaltered level of *Tb*Atm in the former cells and its efficient depletion in the latter ones (Fig. 3D). In the absence of a specific antibody, the downregulation of *Tb*Mdl was followed by quantitative real-time PCR. As shown in Fig. 3E, the *Tb*Mdl mRNA dropped by approximately 70% in the *Tb*Mdl single knockdown, whereas elimination of the same transcript in the *Tb*Atm + *Tb*Mdl double knockdown was even more efficient, lowering it by 85%. Taking into account the limits of RNAi technique, all knockdowns described can be considered efficient.

## *Tb*Atm is required for cytosolic but not mitochondrial Fe-S cluster assembly

To investigate the role of *Tb*Atm in the mitochondrial and cytosolic Fe-S cluster assembly, enzymatic activities of selected Fe-S cluster-containing enzymes have been measured in both cellular compartments. Aconitase is a marker Fe-S protein, in *T. brucei* encoded by a single gene, with approximately 70% and 30% of the protein being targeted to the cytosol and mitochondrion, respectively [44], whereas the studied flagellate encodes in its genome two fumarases: a cytosolic and a mitochondrial one [45]. The dual localization of both enzymes makes them particularly suitable for examining the effects of *Tb*Atm depletion in each compartment of *T. brucei*.

The activities of cytosolic aconitase and fumarase in the *Tb*Atm-depleted cells dropped by 60% and 50%, respectively (Fig. 4A). The unaltered activity of the mitochondrial threonine dehydrogenase was used as a

**Fig. 3.** Separate but not simultaneous depletion of *Tb*Atm and *Tb*Mdl cause growth defect. Growth curves of non-induced (triangles; black line) and RNAi-induced (squares; gray line) cell lines for single *Tb*Atm (A), single *Tb*Mdl (B) and double *Tb*Atm + *Tb*Mdl knockdowns (C). The *y*-axis represents the log scale product of cell density and total dilution. (D) The depletion of *Tb*Atm in each RNAi knockdown was confirmed by western blot analysis, with enolase used as a loading control. (E) Quantitative real-time PCR shows relative *Tb*Mdl mRNA abundance of the single *Tb*Mdl and *Tb*Atm + *Tb*Mdl RNAi-induced cells compared to the non-induced cells.18S rRNA transcript was used as an internal reference.

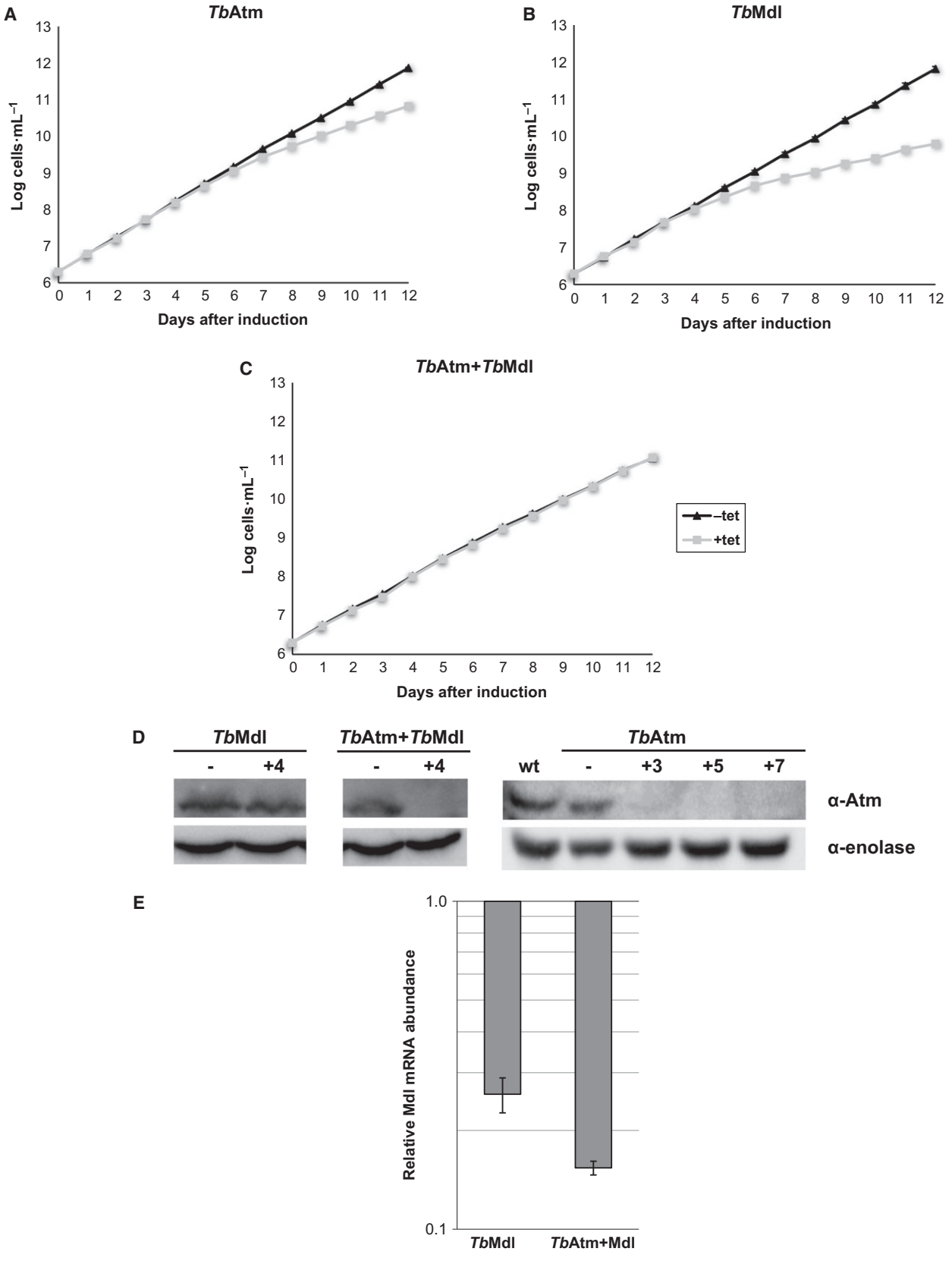
A
*Tb*Atm
Log cells·mL⁻¹
Days after induction
B
*Tb*Mdl
Log cells·mL⁻¹
Days after induction
C
*Tb*Atm+*Tb*Mdl
Log cells·mL⁻¹
Days after induction
–tet
+tet
D
*Tb*Mdl
- +4
*Tb*Atm+*Tb*Mdl
- +4
*Tb*Atm
wt - +3 +5 +7
α-Atm
α-enolase
E
Relative Mdl mRNA abundance
1.0
0.1
*Tb*Mdl
*Tb*Atm+Mdl

Fe-S cluster-lacking control. As in *S. cerevisiae*, *A. thaliana* and humans [24,26], upon the depletion of *Tb*Atm, the activities of both of these enzymes were unaltered in the mitochondrial compartment. As expected, in the PS flagellates downregulated for *Tb*Mdl, neither aconitase, nor fumarase activities were affected in the cytosol and mitochondrion (Fig. 4B). Unexpectedly, when *Tb*Atm and *Tb*Mdl were downregulated at the same time, the enzymatic activities of aconitase and fumarase remained unaltered in both the cytosolic and mitochondrial compartments (Fig. 4C). Again, threonine dehydrogenase remained at wild-type level in each studied cell line, regardless of RNAi induction (Fig. 4).

### *Tb*Atm is required for cytosolic but not mitochondrial tRNA thiolation

Cytosolic tRNA thiolation is fully dependent on a functional mitochondrial ISC assembly pathway [46]. Consequently, by disruption of Atm1, an exporter of the sulfur-containing compound, the levels of cytosolic tRNA thiolation should decrease. A possible link is the histone acetyl transferase Elp3, an Fe-S cluster-containing protein, which plays a crucial role in the formation of the thio-modification $mcm^5s^2U_{34}$ [47]. To assess the effects on tRNA thiolation, cells grown for 7 days in the presence of tetracycline were used for RNA isolation, which was subsequently loaded onto an [(*N*-acryloylamino)-phenyl] mercuric chloride (APM) gel. Under these conditions, sulfur-containing tRNAs migrate slower than their nonthiolated counterparts. Northern blots of APM gels were then probed for the cytosolic $tRNA^{Glu}$ known to be thiolated at the wobble position, and the mitochondrial $tRNA^{Trp}$ which is thiolated at position $U_{33}$. Both cytosolic and mitochondrial tRNAs showed a slowly migrating band indicative of the presence of thiolation. This was confirmed by the disappearance of the slower migrating band upon oxidation with hydrogen peroxide (Fig. 5).

In flagellates downregulated for *Tb*Atm, thiolation of $tRNA^{Glu}$ was reduced by 30%, whereas the mitochondrial $tRNA^{Trp}$ remained fully modified. Importantly,

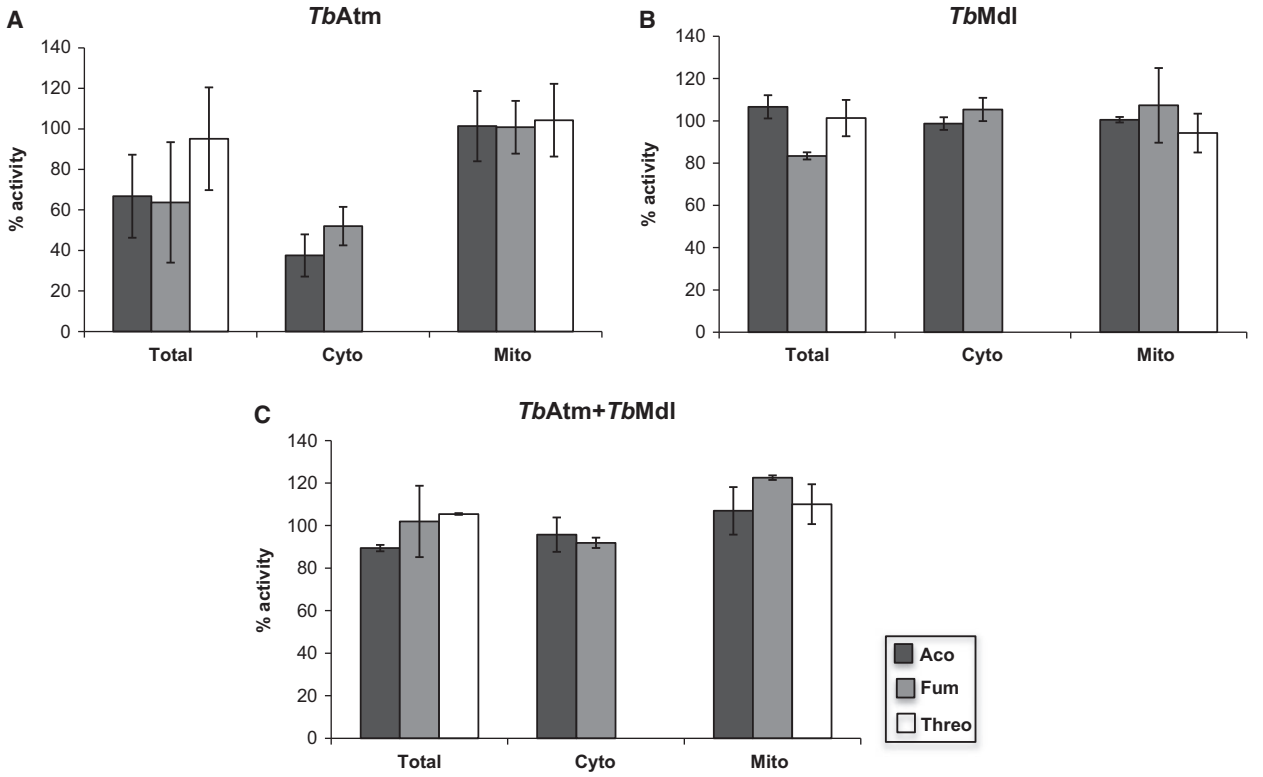


**Fig. 4.** Effect of *Tb*Atm and *Tb*Mdl depletion on Fe-S proteins activities. Enzymatic activities of aconitase (dark gray columns) and fumarase (light gray column) in *Tb*Atm (A), *Tb*Mdl (B) and *Tb*Atm + *Tb*Mdl (C) RNAi-depleted cells were measured in the whole cell lysate (total), cytosolic (cyto) and mitochondrial (mito) fractions. Graphs represent relative percentage of the activities in RNAi-induced compared to the non-induced cells. Enzymatic activity of threonine dehydrogenase (white columns), a non Fe-S protein, was used as a control.

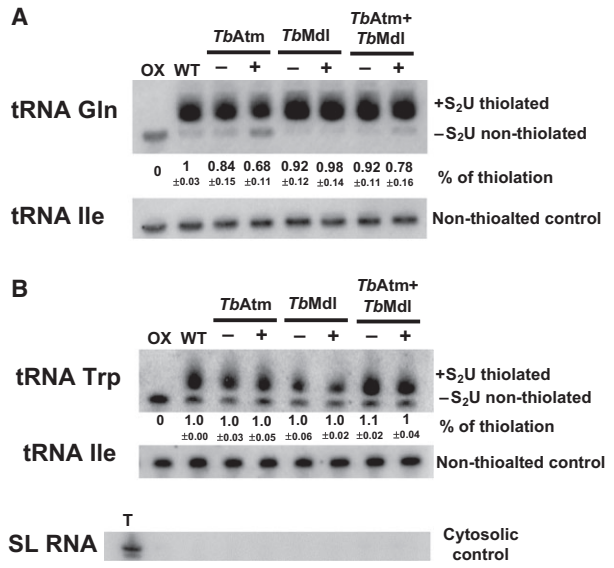


**Fig. 5.** *Tb*Atm is essential for cytosolic but not mitochondrial tRNA thiolation. Cytosolic (A) and/or mitochondrial (B) RNA from wild-type cells (WT) and RNAi-induced cells was separated by APM acrylamide gel electrophoresis and used for Northern blot analysis probing for cytosolic $tRNA^{Gln}$ and mitochondrial $tRNA^{Trp}$, respectively. $H_2O_2$ was used as a control to show complete oxidation of thiolation, eliminating the mobility shift. The $tRNA^{Ile}$ was used as a loading control. Splice leader (SL) RNA show the purity of the mitochondrial fraction. The relative levels of tRNA thiolation are shown below. WT values of tRNA thiolation were set to 1 and the mean ± SE of three independent experiments is shown.

the levels of the nonthiolated cytoplasmic $tRNA^{Ile}$ used as a control were unaltered regardless of the extent of RNAi-mediated *Tb*Atm silencing. In accordance with the measurement of the activities of the cytosolic Fe-S proteins, when *Tb*Mdl is downregulated alone or simultaneously with *Tb*Atm, the level of cytosolic tRNA thiolation remained unaffected or decreased only slightly, respectively (Fig. 5) These data strongly indicate that *Tb*Atm plays an important role in the thiolation of the cytosolic tRNAs (Fig. 5).

## Depletion of *Tb*Atm or *Tb*Mdl does not alter sensitivity to $H_2O_2$

Yeast cells depleted for Atm1 have an increased sensitivity to $H_2O_2$, which is rescued by the overexpression of Mdl1. However, overexpression of the same protein in the wild-type background has an opposite effect because it results in increased $H_2O_2$ sensitivity. This complex picture is further complemented by the Mdl-lacking *S. cerevisiae* being more resistant to the drug [32].

Hence, we decided to study the sensitivity to $H_2O_2$ of wild-type PS trypanosomes, as well as cells in which *Tb*Atm, *Tb*Mdl or *Tb*Atm + *Tb*Mdl were knocked down via RNAi. The cytotoxic effect of $H_2O_2$ was determined by a fluorimetric Alamar blue assay based on the metabolism of resazurin dye. After incubating the flagellates with $H_2O_2$ for 24 h, no significant differences in viability have been detected among the screened cell lines (Fig. 6 and Table 1). We conclude that the depletion of neither *Tb*Atm, nor *Tb*Mdl affects the $H_2O_2$ sensitivity in *T. brucei*.

## Depletion of *Tb*Mdl affects heme content in the mitochondrion

Homologs of Mdl in several eukaryotes have been implicated in heme synthesis [35,48], whereas, for others, such as Mdl2 in *S. cerevisiae*, such a connection remains to be proven. However, because *T. brucei* lost the entire heme synthesis pathway and obtains this tetrapyrrole from the host [38], we decided to test whether *Tb*Mdl plays a role in heme import into its mitochondrion.

Accordingly, the procyclic trypanosomes were cultivated in SDM-79 medium with the addition of 11.4 μM hemin. Heme from the crude mitochondrial fraction, obtained by passing swollen cells in hypotonic solution through a needle, was extracted and analyzed by HPLC. The results show that, contrary to the wild-type procyclic trypanosomes and single *Tb*Atm knockdowns, flagellates depleted for *Tb*Mdl and *Tb*Atm + *Tb*Mdl in parallel have heme *b* decreased in their mitochondrion by approximately 50% and 65%, respectively (Fig. 7). Hence, *Tb*Mdl appears to be a heme *b* importer into the organelle. Additionally, in cells downregulated for either *Tb*Mdl or both *Tb*Atm + *Tb*Mdl, we also detected a marked decrease of heme *a*, which is synthetized from heme *b* in *T. brucei* (Fig. 7). At the same time, we did not detect any accumulation of heme in the cytosol (data not shown) and so we propose that it may be degraded in this compartment.

## *Tb*Atm partially rescues Δ*atm1* in *S. cerevisiae*

The haploid *atm1* null mutant of *S. cerevisiae* is unable to grow on a minimal medium and barely grows on a rich medium [18]. Thus, to investigate whether *Tb*Atm was able to complement the growth defect of *atm1* null mutant in *S. cerevisiae*, a Δ*atm1* diploid strain was generated by the disruption of *ATM1* with the $kan^r$ gene in strain Σ1278b. We

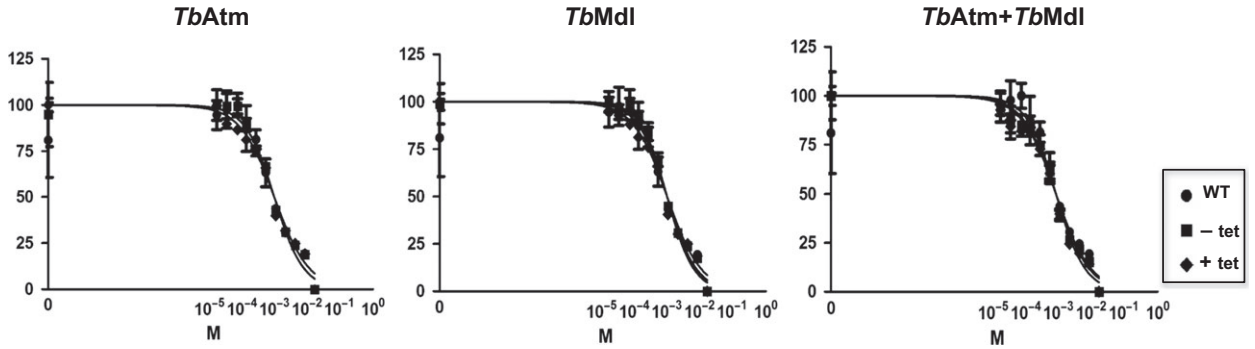


**Fig. 6.** Depletion of *Tb*Atm or *Tb*Mdl does not alter $H_2O_2$ sensitivity. Alamar blue assay was applied to wild-type and *Tb*Atm, *Tb*Mdl and *Tb*Atm + *Tb*Mdl RNAi knockdowns. Fluorescence was read on Tecan using an excitation wavelength of 560 nm and an emission wavelength of 590 nm. The data were analyzed using PRISM software, using the nonlinear regression and sigmoidal dose–response analysis with variable slope to obtain $EC_{50}$ values (Table 1). All experiments were performed in triplicate.

**Table 1.** Sensitivity of RNAi knock-downs to $H_2O_2$.

| Strain | $EC_{50}$ |
|---|---|
| Wild-type | 0.0009457 |
| *Tb*Atm – tet | 0.0009389 |
| *Tb*Atm + tet | 0.0008422 |
| *Tb*Mdl – tet | 0.0010360 |
| *Tb*Mdl + tet | 0.0008377 |
| *Tb*Atm + *Tb*Mdl – tet | 0.0007254 |
| *Tb*Atm + *Tb*Mdl + tet | 0.0006545 |

checked that, upon sporulation, the heterozygous Δ*atm1* exhibits a Mendelian 2 : 2 segregation into a tetrad. Next, yeast *ATM1* and *MDL1*, as well as *Tb*Atm, were separately cloned into the pRS426Met25 (URA3) vector, and the resulting constructs were subsequently introduced into the Δ*atm1* diploid mutant and, after sporulation, haploid cells were grown in a minimal medium lacking uracil. As expected for mutant cells expressing the ectopic copies of yeast *ATM1*, the growth was restored to a wild-type level (Fig. 8A). When the same mutant cells expressed yeast *MDL1*, the growth was partially rescued, which is in agreement with a previous study [32]. Similarly, a complementation with the trypanosome homologue *Tb*Atm was able to support only a limited growth, at approximately the same level as the mutant expressing yeast *MDL1* (Fig. 8A).

### *Tb*Mdl partially rescues Δ*mdl2* in *S. cerevisiae*

The Δ*mdl2* mutant strain of *S. cerevisiae* grows normally in a glucose-rich fermentable medium, whereas it fails to proliferate on nonfermentable sources, such as a glycerol-rich medium. We investigated whether the above-mentioned growth defect of yeast lacking Mdl2 in the BY4742 background (YPL270w; Euroscarf, Frankfurt, Germany) can be rescued by *Tb*Mdl expressed from the high-copy pRS426Met25 vector. As shown in Fig. 8B, in a glucose-rich medium (YPD = 868 medium) the yeast *mdl2* null mutant expressing *Tb*Mdl grows as well as the wild-type cells containing an empty plasmid and the Δ*mdl2* strain, confirming that *Tb*Mdl is not toxic to *S. cerevisiae*. Moreover, expression of the heterologous *T. brucei* protein in the yeast *mdl2* null mutants is able to restore the growth in a glycerol-rich medium, although not to the wild-type level (Fig. 8B).

Simultaneous depletion of Δ*atm1* + Δ*mdl2* in *S. cerevisiae* does not rescue *petite* phenotype of *atm1* single null mutant.

To determine whether the ablation of Mdl2 could partially restore the growth of the *atm1* null mutant, we produced a double Δ*atm1*:Δ*mdl2* mutant from the heterozygous Δ*atm1* diploid strain by disruption of *MDL2* with the nourseothricin-resistance (NAT) gene. Upon sporulation, the heterozygous Δ*atm1* Δ*mdl2* exhibits Mendelian 2 : 2 segregation similar to that observed for the Δ*atm1* cells, although, in this case, only one small colony was observed (Fig. 8C). Segregation analysis of genetic markers checked by replica-plating on YPD agar plate containing G418 and/or NAT revealed that, from more than 10 ascii dissected from two different sporulations, all small colonies (*petite* phenotype) correspond to the single atm1 null mutants, whereas the colonies that did not grow appear to correspond to the double mutants (NAT and G418-resistant) (data not shown). Thus, in contrast to that observed in *T. brucei* in the double *Tb*Atm + *Tb*Mdl knockdown, in yeast, the ablation of both transporters leads to a synthetic lethal phenotype.

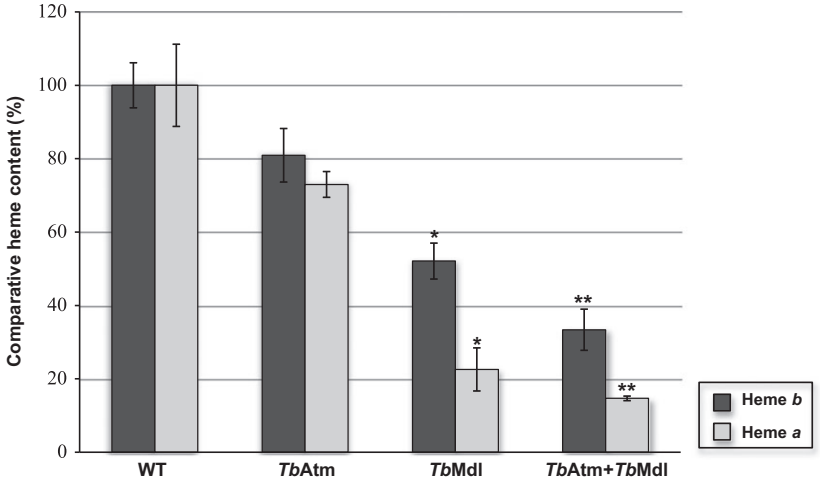


**Fig. 7.** Depletion of *Tb*Mdl affects heme content in the mitochondrion. The amount of heme *a* (light gray) and heme *b* (dark gray) is shown as a percentage with the level in the wild-type (WT) cells set to 100%. The mean ± SD of three independent RNAi-inductions is shown. Heme was extracted from crude mitochondrial vesicles isolated from $1 \times 10^9$ wild-type and RNAi-induced cells (day 6 post-induction), separated by HPLC and detected by diode array detector. Data were analyzed by Student's *t*-test for independent samples, using PRISM software. $*P < 0.05$, $**P < 0.001$.

## Discussion

Despite extensive research, we still do not fully understand the precise function of individual mitochondrial ABC transporters and the way that they cooperate to establish the homeostasis of the essential cofactors in and out of the organelle. It is well known that Atm1 plays a critical role in Fe-S cluster assembly in the cytosol, although the nature of the compound transported from the mitochondrion is still debated and remains enigmatic [3].

It has been proposed that yeast Mdl1 and its homolog in *Caenorhabditis elegans* serve as exporters of proteolytic oligopeptides resulting from misfolded proteins outside the mitochondrial matrix [30,49]. In most eukaryotes, the only homologue of Mdl is ABCB10, which was recently postulated to export delta-aminolevulinic acid from mitochondria into the cytosol of cardiac cells [35], whereas, in differentiated mouse erythroleukemia cells, it interacts with Mfrn1 to stabilize and promote heme import into the organelle [33]. A transient interaction between the ABCB10-Mfrn1 complex and ferrochelatase [34] needs to be investigated further, yet it represents an additional link of Mdl with heme metabolism. Furthermore, the absence of ABCB10 causes accumulation of protoporphyrin IX, an intermediate in the last step of heme synthesis [48]. Collectively, these studies support the view that ABCB10 is involved in heme homeostasis.

*Trypanosoma brucei* is a heme auxotroph that lost all enzymes of the heme biosynthesis pathway [38]. The parasite must acquire heme from its host, and heme receptors capable of such activity have been characterized [50]. Yet, how the flagellate delivers heme to its single reticulated mitochondrion remains unknown. We therefore considered whether *Tb*Mdl or *Tb*Atm play a role in heme import into the mitochondrion of *T. brucei*. Our data indeed support such a function because the content of heme *b* and *a* dropped to varying extent in the mitochondrion of flagellates depleted for *Tb*Mdl. We have observed the same phenotype in flagellates depleted for both *Tb*Atm and *Tb*Mdl proteins, with the decrease of both hemes being even more pronounced. On the other hand, the amount of heme *a* and *b* in single *Tb*Atm knockdown was not significantly changed, suggesting that it may be involved in heme homeostasis indirectly. All together, our data strongly suggest a role of *Tb*Mdl in import of heme *b* into the organelle and/or heme *a* biosynthesis.

As a result of general similarities between the phenotypes after the depletion of Atm1 and Erv1 in *S. cerevisiae* [20,21], we considered whether the massive mitochondrial swelling observed in *T. brucei* upon downregulation of *Tb*Erv1 [43] will also occur in the *Tb*Atm-depleted cells. However, no alteration in organellar morphology was observed (data not shown), strongly indicating that the relationship between these proteins, in the marked absence of Mia40 [43,51], may be different in *T. brucei*. Both *Tb*Atm and *Tb*Mdl contain a mitochondrial targeting sequence, transmembrane and nucleotide-binding domains, and have been previously found as components of the PS mitochondrial proteome [41]. For *Tb*Atm, we have confirmed localization in the organelle by immunofluorescence microscopy using the GFP-tagging strategy. For functional analysis, single and double RNAi knockdowns of the PS cells have been generated.

In *S. cerevisiae*, *Δatm1* results in a *petite* phenotype capable of growth on a minimal medium [18]. In *A. thaliana*, *At*ATM3 deficiency causes a host of defects in chlorophyll content, seed establishment,

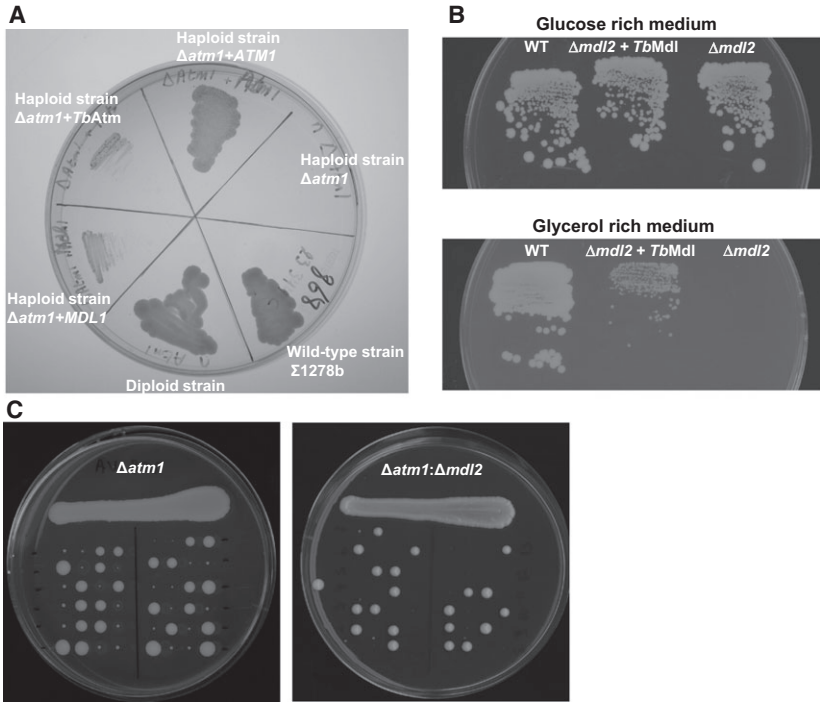


**Fig. 8.** Complementation of *Tb*Atm and *Tb*Mdl in *S. cerevisiae*. (A) Viability of *S. cerevisiae atm1* null haploid strain (haploid strain Δ*atm1*), wild-type, *ATM1* single allele-deleted diploid strain (diploid strain *ATM1*/*atm1*), *atm1* null haploid strain expressing yeast *MDL1* (haploid strain Δ*atm1* + *MDL1*), *atm1* null haploid strain expressing *Tb*Atm (haploid strain Δ*atm1* + *Tb*Atm) and *atm1* null haploid strain expressing yeast *ATM1* (haploid strain Δ*atm1* + *ATM1*). Cells were grown on synthetic minimal medium lacking uracil and methionine. (B) *S. cerevisiae* wild-type (WT), *mdl2* null expressing *Tb*Mdl (Δ*mdl2* + *Tb*Mdl) and *mdl2* null mutant with empty pRS426Met vector (Δ*mdl2*) were grown on a glucose-rich medium (fermentable carbon source; upper) and a glycerol-rich medium (nonfermentable carbon source; lower). (C) Haploid disruptants from both diploid heterozygous Δ*atm1* and Δ*atm1* Δ*mdl2* mutants. After sporulation of a diploid strain with one copy of ATM1 disrupted by insertion of the KanMX, 12 tetrads were dissected on 868 medium plate incubated for 7 days at 30 °C. All tetrads present the Mendelian 2 : 2 segregation. Additional disruption of the *MDL2* gene by NAT in the diploid heterozygous Δ*atm1* was sporulated and 12 tetrads were dissected and incubated for 5 days at 30 °C. Although all slow-growing spores were G418 resistant (Δ*atm1* null mutants), the largest spores were either WT (ATM1/MDL2) or NAT resistant (ATM1/Δ*mdl2*). No resistance to both NAT and G418 was observed, suggesting that the haploid double mutant exhibits synthetic lethality.

decreased root growth and dwarfism [26,52]. Because mutations in ABCB7 in humans cause X-linked sideroblastic anemia with ataxia [23], it is obvious that at least one Atm homologue is essential for each of these model organisms. Moreover, cross-complementation studies confirmed that human ABCB7 and *A. thaliana* *At*ATM3 and, to lesser extent, *At*ATM1, are able to rescue not only growth defect in the yeast Δ*atm1*, but also suppress mitochondrial iron accumulation and restore respiration and activities of the cytosolic Fe-S proteins [23,25]. Similarly, the overexpression of yeast Mdl1 partially complemented growth defect and reduced iron accumulation in the mitochondria of Δ*atm1 S. cerevisiae* [32].

Given the general essentiality of Atm1, the relatively mild growth phenotype caused by its efficient down-regulation in *T. brucei* was rather unexpected, especially when the depletion of *Tb*Mdl led to a more pronounced growth defect. This latter phenotype is not unexpected because deletion of ABCB10, its mammalian homolog, caused death of mouse embryos by day 12, as a consequence of increased reactive oxygen species, mitochondrial protein oxidation and apoptosis [53]. ABCB10 was proposed to export delta-aminolevulinic acid, an early precursor of heme synthesis, from the human mitochondrion [35], yet, because of the lack of a heme synthesis pathway in *T. brucei* [38,54], such a function is impossible in this parasitic protist. There is also another putative *Tb*Mdl homologue in mammals called ABCB8 with high sequence similarity (77%), which is predicted to be involved in the compartmentalization and transport of heme, as well as peptides, from the mitochondrion.

As a result of the position of the export machinery connecting the cytosolic and mitochondrial Fe-S cluster biogenesis, processes upstream of Atm1 should not

be affected upon its depletion. Indeed, in the procyclic trypanosomes missing *Tb*Atm, activities of the Fe-S cluster-containing mitochondrial aconitase and fumarase remained unaltered. By contrast, activities of the same enzymes located in the cytosol were substantially decreased. This result confirms the notion that maturation of the cytosolic Fe-S clusters depends, at least to some extent, on the mitochondrial ISC machinery and that Atm1 is an important link between both cellular compartments [1,55]. Furthermore, the ability of *Tb*Atm to partially complement the growth defect of the yeast knockdown is in line with this interpretation. No significant changes in the enzymatic activities of fumarase and aconitase in both compartments were observed in the *Tb*Mdl-depleted cells, strongly indicating that this protein does not have a direct role in the Fe-S cluster biogenesis.

Unexpectedly, the simultaneous depletion of *Tb*Atm and *Tb*Mdl did not cause any growth phenotype, even though single RNAi knockdowns of each gene resulted in an altered growth. Furthermore, the enzymatic activities of aconitase and fumarase in the cytosolic and mitochondrial compartments were unaltered, in contrast with results obtained after the sole elimination of *Tb*Atm.

The Urm1 pathway is responsible for the 2-thiolation of $mcm^5s^2U_{34}$ in the cytosol of eukaryotes. The formation of 2-thiouridine thiolation requires functional mitochondrial ISC and CIA machineries in yeast, as well as in trypanosomes [46,56]. This suggests that the cytosolic thiolation, unlike the mitochondrial one, contains a Fe-S protein. Therefore, we also tested levels of the cytosolic and mitochondrial tRNA thiolation in all RNAi cell lines. In the present study, we show for the first time that the downregulation of *Tb*Atm affects thiolation of the cytosolic tRNAs in *T. brucei*, whereas mitochondrial 2-thiouridine formation remains unaffected. Silencing of *Tb*Mdl did not change thiolation levels in both the cytosol and the organelle. In line with other data reported here, simultaneous downregulation of *Tb*Atm and *Tb*Mdl restores thiolation close to the wild-type levels.

*Tb*Atm is clearly needed for the cytosolic Fe-S cluster assembly and tRNA thiolation. This result is highly reproducible, allowing the conclusion that, in the background of concurrently missing *Tb*Mdl, *Tb*Atm is no longer indispensable for the maturation of Fe-S cluster and, consequently, for tRNA thiolation in the cytosol. The lack of growth phenotype of cells downregulated for *Tb*Atm and *Tb*Mdl can be explained by the excess/deficiency of substrates in different cellular compartments (Fig. 9). As demonstrated in the present study, *Tb*Mdl appears to have a role in heme metabolism by transporting the heme inside the mitochondrion where it is needed the most, serving as a cofactor for several cytochromes. If this route is closed and heme is forced to stay in the cytosol, it may be degraded there (Fig. 9). From *Plasmodium*, it is known that, under certain conditions, heme is degraded by glutathione. By this action, glutathione is being oxidized to glutathione disulfide, which leads to shifted glutathione disulfide/glutathione ratio, the hallmark of oxidative stress [57]. At this point, we can only speculate that similar detoxification mechanism may be present in trypanosomes, which contain a specialized form of thiol called trypanothione [58]. Interestingly, the trypanothione reductase is present only in the cytosol [59] and so the oxidized thiol needs to exit the mitochondrion to be reduced and maintain the cellular redox balance. Here, Atm may be very important because it is implicated in transport of glutathione polysulfide from the mitochondrion [28]. Further studies are needed to shed more light on this intriguing possibility.

## Experimental procedures

### Phylogenetic analysis

The representative datasets of Mdl and Atm1 amino acid sequences covering the known eukaryotic diversity were extracted from public databases (GenBank, JGI, TriTrypDB) using a homology search (BLAST). Sequences were aligned with MAFFT [60] and the ambiguously aligned regions were manually removed in SEAVIEW 4 [61]. Maximum likelihood phylogeny of the aligned dataset was created using RAXML 8.1a [62], employing a Γ-corrected LG4X model. The highest scoring topology was chosen from 100 independent runs, each starting with a different starting tree. Branching support was assessed using nonparametric bootstrapping (RAXML LG4X + Γ; 500 replicates).

### Intracellular localization by in situ GFP-tagging of endogenous *Tb*Atm

To generate a PS cell line expressing C-terminal GFP chimera of *Tb*Atm protein, two DNA fragments of approximately 300 bp corresponding to the 3′ end of the endogenous Tb927.11.16930 ORF sequence (minus the stop codon) and the immediate 3′ UTR were amplified by PCR using primers containing, respectively, *Xho*I/*Spe*I and *Hind*III/*Xho*I restriction sites. Resulting DNA fragments were simultaneously ligated into pET-GFP (Hyg) using the *Hind*III and *Spe*I sites of the vector [42]. The resulting construct was linearized by *Xho*I and transfected into the *T. brucei* ProAnv PS cell line. Stable transformants expressing the endogenously GFP-tagged *Tb*Atm gene were selected using hygromycin (50 $\mu g \cdot mL^{-1}$).

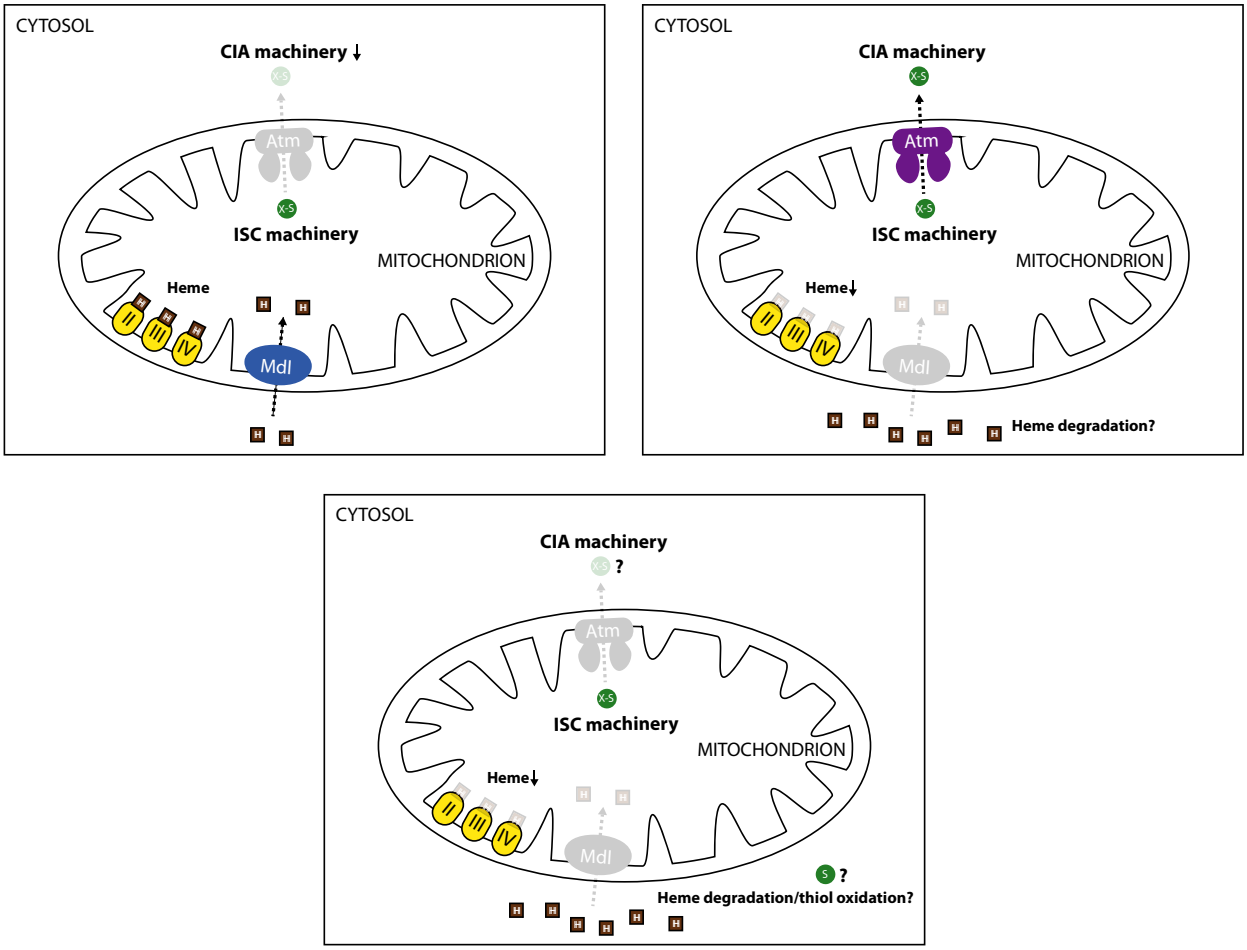


**Fig. 9.** Schematic illustration of putative relationships of *Tb*Atm and *Tb*Mdl and their substrates in *T. brucei* after their individual and simultaneous RNAi-mediated depletions.

## Generation of *Tb*Atm, *Tb*Mdl and *Tb*Atm + *Tb*Mdl RNAi cell lines and cultivation

Using genomic DNA of *T. brucei* strain 29–13 as a template, 546 and 450-nucleotide long fragments of the *Tb*Atm and *Tb*Mdl genes, respectively, were amplified by primer pairs TbAtm1RI-F (5′-CGAAGCTTACATTGCGTTCGT GTGCG-3′) and TbAtm1RI-R (5′-CGTGGATCCCCAA AATGGCACTGCCAC)-3′ (added *Hind*III and *BamH*I restriction sites are underlined) and TbMdlRI-F (5′-GCACTCGAGTCTCGCCACTTTACGTTGTG-3′) and TbMdlRI-R (5′-CGTAAGCTTCGCGCCAATAAGGT TACAAT-3′) (added *Xho*I and *Hind*III restriction sites are underlined). Both amplicons were separately cloned into the opposing tetracycline-regulatable promoter-containing p2T7-177 vector. Upon *Not*I-mediated linearization, the vector was introduced into the PS *T. brucei* 29–13 cells using a BTX electroporator (Harvard Apparatus, Inc., Holliston, MA, USA) and selected as described previously [63]. The double RNAi knockdown was prepared by cloning the same fragment of the *Tb*Mdl gene plus part of *Tb*Atm gene into the p2T7-177, which was stably integrated into the same cell line. The PS flagellates were cultivated in SDM-79 medium containing appropriate antibiotics at 27 °C. Downregulation by RNAi was induced by the addition of 1 μg·mL$^{-1}$ tetracycline to the medium. Cell density was measured every 24 h using the Z2 counter (Beckman Coulter, Fullerton, CA, USA).

## Western blot analysis

Polyclonal antibodies against *Tb*Atm were prepared by immunizing a rabbit with synthetic oligopeptide CKDQEQ-WEPSKKPDIV by Eurogentec (Liège, Belgium). Cell lysates corresponding to 5 × 10$^6$ cells per lane were separated on 12% SDS/PAGE and the proteins were subsequently transferred to a poly(vinylidene difluoride) membrane. The membrane was hybridized using the anti-*Tb*Atm and enolase antibodies (with the latter kindly

provided by Paul A. M. Michels) at dilutions of 1 : 500 and 1 : 200 000, respectively. After hybridizing with an appropriate secondary antibody conjugated with horseradish peroxidase (Sigma, St Louis, MO, USA), the ELC kit was used to visualize protein bands on the membrane.

## Quantitative real-time PCR

Total RNA was isolated using TRIzol (Sigma) and residual DNA was removed by the turbo DNA-free DNase kit (Ambion, Austin, TX, USA). To obtain cDNA, reverse transcription using the SuperScript III reverse transcriptase (Invitrogen, Carlsbad, CA, USA) with oligo $(dT)_{20}$ primer (Invitrogen) was performed. Quantitative real-time PCR reactions were performed as described previously [64]. For the detection of *Tb*Mdl mRNA, primer pair *Tb*Mdl-qF (5′-GACTGGGATGATGCGGTTGATC-3′) and *Tb*Mdl-qR (5′-GTCAAGTGCAGATGTGGCTTCAT-3′) was used. The 18S rRNA gene, used as an internal reference, was followed as reported previously [65]. The relative *Tb*Mdl mRNA abundance in the non-induced and RNAi-induced cells was determined by the Pfaffl method [66].

## Digitonin fractionation and enzymatic activities measurement

The subcellular cytosolic and mitochondrial fractions were obtained by digitonin fractionation as described previously [67]. In each cell fraction, enzymatic activities were measured spectrophotometrically at either 240 nm (aconitase and fumarase) or 340 nm (threonine dehydrogenase) in accordance with the protocols described previously [44,64].

## Heme measurement

The PS cells were cultivated in SDM-19 medium without the addition of hemin. For the measurement of heme in whole PS flagellates, a total of $5 \times 10^8$ cells was harvested and washed three times with PBS. For establishing heme levels in the mitochondrion, the crude mitochondrial fraction was isolated from $1 \times 10^9$ cells in accordance with a protocol described elsewhere [68]. The pellet was resuspended in 60 μL of $H_2O$ and extracted with 400 μL of acetone/0.2% HCl. The supernatant was then collected after centrifugation at 9660 ***g*** for 5 min. The pellet was resuspended in 200 μL of acetone/0.2% HCl and centrifuged again for 5 min at 9660 ***g*** Both supernatants were combined and 150 μL of each sample was injected into an HPLC 1200 machine (Agilent Technologies Inc., Santa Clara, CA, USA) and separated using a reverse phase column (4 μm particle size, 3.9 × 75 mm; Waters, Milford, MA, USA) with 0.1% trifluoroacetic acid and acetonitrile/0.1% trifluoroacetic acid as solvents A and B, respectively. The total heme was eluted with a linear gradient of solvent B (30–100% in 12 min) followed by 100% of B at a flow rate of 0.8 $mL \cdot min^{-1}$ at 40 °C. Heme *a* and *b* were separately detected by diode array detector 1200 (Agilent Technologies) and identified by retention time and absorbance spectra according to commercially available standards (Sigma, Darmstadt, Germany).

## Cell viability measurement via Alamar blue assay

$H_2O_2$ was dissolved in SDM-79 medium and subsequently distributed to a 96-wells plate with a two-fold serial dilution. Each well contained 50 μL and one well in each row was left without the addition of $H_2O_2$, serving as a blank. Next, 50 μL of $2 \times 10^5$ cells were added to each well, resulting in the final concentration of $H_2O_2$ in the range 0.0156–16 mM. The plate was incubated for 1 h at 27 °C and then 10 μL of resazurin (1.25 $mg \cdot mL^{-1}$ in PBS) was added. The plate was then incubated at 27 °C for 24 h, after which the fluorescence was read by Infinite M200 pro-reader (Tecan, Austria GmbH, Grödig, Austria) using excitation and emission wave lengths of 560 and 590 nm, respectively. The data was analyzed using PRISM (GraphPad Software Inc., San Diego, CA, USA) using the nonlinear regression and sigmoidal dose–response analysis.

## Yeast strains and growth conditions

The *S. cerevisiae* strains used in the present study are isogenic to either Σ1278b strain used as wild-type [69] to construct the Δ*atm1* mutant or BY4742 strain for the Δ*mdl2* mutant (MATα, his3Δ1, leu2Δ0, lys2Δ0, ura3Δ0, YPL270w::KanMX4) obtained from Euroscarf (YPL270w). Cells were grown on 1% yeast extract, 2% bactopeptone supplemented with 2% glucose (YPD) or 3% glycerol (YPG). For selective growth, yeast cells were cultivated in a minimal buffered medium [70] containing nitrogen sources (10 mM $[NH_4]_2SO_4$, 0.1% proline, 0.1% citrulline and 0.1% urea), as well as 3% glucose as a carbon source supplemented with leucine, histidine, lysine and uracil in accordance with the auxotrophic requirements. Yeast cells were treated with lithium acetate and transformed according to [71].

## Construction of yeast Δ*atm1* mutant

For construction of a diploid heterozygous *ATM1*/*atm1*Δ::URA3 mutant, we first replaced by homologous recombination the entire *ATM1* coding sequence by a PCR product expressing the geneticin resistance gene (kanMX marker) and containing 40 bp extensions homologous to endogenous *ATM1* [72]. A DNA fragment was amplified with the primers MET25Atm1 (5′-GTCAGATACATAGATA CAATTCTATTACCCCCATCCATACATGCTGCTTCTT CCAAGATG-3′) and CYC1Atm1 5′-GGGAGGGCGTGA

ATGTAAGCGTGACATAACTAATTACATGATCATA GTTCTTGCTGGTCTT-3′. The obtained PCR product was used to transform the isogenic diploid strain Σ1278b. Correct integration of the construct was checked using PCR with primers complementary to 5′ and 3′ UTR from *ATM1*. Two transformed clones that contained both the wild-type and the disrupted allele were sporulated on minimum medium containing 1% potassium acetate to check the Mendelian 2 : 2 segregation.

### Complementation assay in yeast

For the complementation assays, wild-type *ATM1*, *MDL1*, *MDL2* and *Tb*Atm were expressed in a high-copy number 2-micron plasmid (pRS426 under the control of the MET25 promoter and CYC1 terminator) with a *URA3* marker that were constructed in yeast by PCR-directed *in vivo* plasmid construction by homologous recombination using, respectively, the following primers, MET25Atm1 (5′-GTCAGATACATAGATACAATTCTATTACCCCCA TCCATACATGCTGCTTCTTCCAAGATG-3′) and CYC 1Atm1: (5′-GGGAGGGCGTGAATGTAAGCGTGACA TAACTAATTACATGATCATAGTTCTTGCTGGTCTT 3′); MET25*Tb*Atm1 (5′-GTCAGATACATAGATACAATT CTATTACCCCCATCCATACATGCGGCGCGCTGCGT TCTGT-3′) and CYC1*Tb*Atm1 (5′-GGGAGGGCGTGAA TGTAAGCGTGACATAACTAATTACATGACTACTCC TCAGCACGATGTGC-3′); MET25*Tb*Mdl2 (5′- to 3′) and *CYC1TbMdl2* (5′- to 3′); MET25Mdl1 (5′-GTCAGATA CATAGATACAATTCTATTACCCCCATCCATACATG ATTGTAAGAATGATACG-3′) and CYC1Mdl1 (5′-GGG AGGGCGTGAATGTAAGCGTGACATAACTAATTAC ATGATTATACTTCCCGGGCAACAC-3′). The resulting constructs expressing *ATM1*, *Tb*Atm and *MDL1* were subsequently used to transform the Δ*atm1* diploid mutant and incubated in complete medium and then cloned on YPD agar containing methionine and lacking uracil. Several clones from each transformation were sporulated, and haploid cells were grown in minimal medium lacking uracil and methionine. The construct expressing *Tb*Mdl was used to transform the Δ*mdl2* haploid mutant and cloned on synthetic dextrose minimal medium containing the auxotrophic markers histidine, leucine, lysine and lacking uracil.

### Thiolation of tRNAs

Thiolation of different tRNAs was analyzed using the APM gel, and blotted as described previously [73]. In the control reactions, the thiol group was removed by treatment with 0.4% hydrogen peroxide, 1 mM EDTA and 100 mM phosphate buffer (pH 8.0) for 1 h at room temperature. The percentage of thiolation was established using the volume of band(s) corresponding to the thiolated and nonthiolated species and calculated as described previously [56].

## Acknowledgements

We thank Shaojun Long (Washington University School of Medicine, St Louis) and Aurélie Wertz (Université Libre de Bruxelles, Gosselies) for the initial experiments; Aleš Horák (Biology Centre, České Budějovice) for phylogenetic analysis; Roman Sobotka (Institute of Microbiology, Třeboň) for heme measurement; Luděk Kořený (Cambridge University, Cambridge) for discussions; Bruno André and Catherine Jauniaux (Université Libre de Bruxelles, Gosselies) for advice and help with yeast experiments; and Paul A. M. Michels (Universidad de los Andes, Mérida/University of Edinburgh, Edinburgh) for the gift of α-enolase antibody. This work was supported by the Czech Grant Agency (P305/11/2179; 15-21450Y); the Wallonie-Bruxelles International (WBI)/ Coordenação de Aperfeiçoamento de Pessoal de Nível Superior (CAPES) bilateral cooperation agreement; the Czech Ministry of Education (AMVIS LH12104); and the Praemium Academiae award to J.L. We acknowledge the use of research infrastructure that has received funding from the European Union Seventh Framework Programme (FP7/2007-2013) under grant agreement no. 316304.

## Author contribution

EvaHoráková-Planned experiments; Performed experiments; Analyzed data; Wrote the paper. Piya Changmai-Performed experiments; Analyzed data; Wrote the paper. Zdenek Paris-Performed experiments; Analyzed data. Didier Salmon-Performed experiments; Analyzed data. Julius Lukes-Planned experiments, provided financial support; Wrote the paper.

## References

1 Lill R (2009) Function and biogenesis of iron-sulphur proteins. *Nature* **460**, 831–838.
2 Netz DJA, Stith CM, Stümpfig M, Köpf G, Vogel D, Genau HM, Stodola JL, Lill R, Burgers PMJ & Pierik AJ (2012) Eukaryotic DNA polymerases require an iron-sulfur cluster for the formation of active complexes. *Nat Chem Biol* **8**, 125–132.
3 Lill R, Srinivasan V & Mühlenhoff U (2014) The role of mitochondria in cytosolic-nuclear iron–sulfur protein biogenesis and in cellular iron regulation. *Curr Opin Microbiol* **22**, 111–119.
4 Zheng L, White RH, Cash VL, Jack RF & Dean DR (1993) Cysteine desulfurase activity indicates a role for NIFS in metallocluster biosynthesis. *Proc Natl Acad Sci USA* **90**, 2754–2758.
5 Kakuta Y, Horio T, Takahashi Y & Fukuyama K (2001) Crystal structure of *Escherichia coli* Fdx, an

adrenodoxin-type ferredoxin involved in the assembly of iron-sulfur clusters. *Biochemistry* **40**, 11007–11012.
6 Yoon T & Cowan JA (2003) Iron-sulfur cluster biosynthesis. Characterization of frataxin as an iron donor for assembly of [2Fe-2S] clusters in ISU-type proteins. *J Am Chem Soc* **125**, 6078–6084.
7 Kondapalli KC, Kok NM, Dancis A & Stemmler TL (2008) *Drosophila* frataxin: an iron chaperone during cellular Fe-S cluster bioassembly. *Biochemistry* **47**, 6917–6927.
8 Bedekovics T, Gajdos GB, Kispal G & Isaya G (2007) Partial conservation of functions between eukaryotic frataxin and the *Escherichia coli* frataxin homolog CyaY. *FEMS Yeast Res* **7**, 1276–1284.
9 Adinolfi S, Iannuzzi C, Prischi F, Pastore C, Iametti S, Martin SR, Bonomi F & Pastore A (2009) Bacterial frataxin CyaY is the gatekeeper of iron-sulfur cluster formation catalyzed by IscS. *Nat Struct Mol Biol* **16**, 390–396.
10 Mühlenhoff U, Gerl MJ, Flauger B, Pirner HM, Balser S, Richhardt N, Lill R & Stolz J (2007) The iron-sulfur cluster proteins Isa1 and Isa2 are required for the function but not for the *de novo* synthesis of the Fe/S clusters of biotin synthase in *Saccharomyces cerevisiae*. *Eukaryot Cell* **6**, 495–504.
11 Long S, Changmai P, Tsaousis AD, Skalický T, Verner Z, Wen YZ, Roger AJ & Lukeš J (2011) Stage-specific requirement for Isa1 and Isa2 proteins in the mitochondrion of *Trypanosoma brucei* and heterologous rescue by human and *Blastocystis* orthologues. *Mol Microbiol* **81**, 1403–1418.
12 Sheftel AD, Wilbrecht C, Stehling O, Niggemeyer B, Elsasser H-P, Mühlenhoff U & Lill R (2012) The human mitochondrial ISCA1, ISCA2, and IBA57 proteins are required for [4Fe-4S] protein maturation. *Mol Biol Cell* **23**, 1157–1166.
13 Tong WH & Rouault TA (2006) Functions of mitochondrial ISCU and cytosolic ISCU in mammalian iron-sulfur cluster biogenesis and iron homeostasis. *Cell Metab* **3**, 199–210.
14 Biederbick A, Stehling O, Rösser R, Niggemeyer B, Nakai Y, Elsässer H-P & Lill R (2006) Role of human mitochondrial Nfs1 in cytosolic iron-sulfur protein biogenesis and iron regulation. *Mol Cell Biol* **26**, 5675–5687.
15 Chloupková M, Reaves SK, LeBard LM & Koeller DM (2004) The mitochondrial ABC transporter Atm1p functions as a homodimer. *FEBS Lett* **569**, 65–69.
16 Kispal G, Csere P, Prohl C & Lill R (1999) The mitochondrial proteins Atm1p and Nfs1p are essential for biogenesis of cytosolic Fe/S proteins. *EMBO J* **18**, 3981–3989.
17 Teschner J, Lachmann N, Schulze J, Geisler M, Selbach K, Santamaria-Araujo J, Balk J, Mendel RR & Bittner F (2010) A novel role for *Arabidopsis* mitochondrial ABC transporter ATM3 in molybdenum cofactor biosynthesis. *Plant Cell* **22**, 468–480.
18 Leighton J & Schatz G (1995) An ABC transporter in the mitochondrial inner membrane is required for normal growth of yeast. *EMBO J* **14**, 188–195.
19 Miao R, Kim H, Koppolu UMK, Ellis EA, Scott RA & Lindahl PA (2009) Biophysical characterization of the iron in mitochondria from Atm1p-depleted *Saccharomyces cerevisiae*. *Biochemistry* **48**, 9556–9568.
20 Sipos K, Lange H, Fekete Z, Ullmann P, Lill R & Kispal G (2002) Maturation of cytosolic iron-sulfur proteins requires glutathione. *J Biol Chem* **277**, 26944–26949.
21 Kumar C, Igbaria A, D'Autreaux B, Planson A-G, Junot C, Godat E, Bachhawat AK, Delaunay-Moisan A & Toledano MB (2011) Glutathione revisited: a vital function in iron metabolism and ancillary role in thiol-redox control. *EMBO J* **30**, 2044–2056.
22 Taketani S, Kakimoto K, Ueta H, Masaki R & Furukawa T (2003) Involvement of ABC7 in the biosynthesis of heme in erythroid cells: Interaction of ABC7 with ferrochelatase. *Blood* **101**, 3274–3280.
23 Bekri S, Kispal G, Lange H, Fitzsimons E, Tolmie J, Lill R & Bishop DF (2000) Human ABC7 transporter: gene structure and mutation causing X-linked sideroblastic anemia with ataxia with disruption of cytosolic iron-sulfur protein maturation. *Blood* **96**, 3256–3264.
24 Cavadini P, Biasiotto G, Poli M, Levi S, Verardi R, Zanella I, Derosas M, Ingrassia R, Corrado M & Arosio P (2007) RNA silencing of the mitochondrial ABCB7 transporter in HeLa cells causes an iron-deficient phenotype with mitochondrial iron overload. *Blood* **109**, 3552–3559.
25 Chen S, Sánchez-Fernández R, Lyver ER, Dancis A & Rea PA (2007) Functional characterization of AtATM1, AtATM2, and AtATM3, a subfamily of *Arabidopsis* half-molecule ATP-binding cassette transporters implicated in iron homeostasis. *J Biol Chem* **282**, 21561–21571.
26 Bernard DG, Cheng Y, Zhao Y & Balk J (2009) An allelic mutant series of ATM3 reveals its key role in the biogenesis of cytosolic iron-sulfur proteins in *Arabidopsis*. *Plant Physiol* **151**, 590–602.
27 Srinivasan V, Pierik AJ & Lill R (2014) Crystal structures of nucleotide-free and glutathione-bound mitochondrial ABC transporter Atm1. *Science* **343**, 1137–1140.
28 Schaedler TA, Thornton JD, Kruse I, Schwarzländer M, Meyer AJ, van Veen HW & Balk J (2014) A conserved mitochondrial ATP-binding cassette transporter exports glutathione polysulfide for cytosolic metal cofactor assembly. *J Biol Chem* **289**, 23264–23274.
29 Lee JY, Yang JG, Zhitnitsky D, Lewinson O & Rees DC (2014) Structural basis for heavy metal

detoxification by an Atm1-type ABC exporter. *Science* **343**, 1133–1136.
30 Young L, Leonhard K, Tatsuta T, Trowsdale J & Langer T (2001) Role of the ABC transporter Mdl1 in peptide export from mitochondria. *Science* **291**, 2135–2138.
31 Hofacker M, Gompf S, Zutz A, Presenti C, Haase W, van der Does C, Model K & Tampé R (2007) Structural and functional fingerprint of the mitochondrial ATP-binding cassette transporter Mdl1 from *Sacharomyces cerevisiae*. *J Biol Chem* **282**, 3951–3961.
32 Chloupková M, LeBard LS & Koeller DM (2003) MDL1 is a high copy suppressor of ATM1: evidence for a role in resistance to oxidative stress. *J Mol Biol* **331**, 155–165.
33 Chen W, Paradkar PN, Li L, Pierce EL, Langer NB, Takahashi-Makise N, Hyde BB, Shirihai OS, Ward DM, Kaplan J *et al*. (2009) Abcb10 physically interacts with mitoferrin-1 (Slc25a37) to enhance its stability and function in the erythroid mitochondria. *Proc Natl Acad Sci USA* **106**, 16263–16268.
34 Chen W, Dailey HA & Paw BH (2010) Ferrochelatase forms an oligomeric complex with mitoferrin-1 and Abcb10 for erythroid heme biosynthesis. *Blood* **116**, 628–630.
35 Bayeva M, Khechaduri A, Wu R, Burke MA, Wasserstrom JA, Singh N, Liesa M, Shirihai OS, Langer NB, Paw BH *et al*. (2013) ATP-binding cassette B10 regulates early steps of heme synthesis. *Circ Res* **113**, 279–287.
36 Panek H & Brian MRO (2002) A whole genome view of prokaryotic haem biosynthesis. *Microbiology* **148**, 2273–2282.
37 Moraes CT, Diaz F & Barrientos A (2004) Defects in the biosynthesis of mitochondrial heme c and heme a in yeast and mammals. *Biochim Biophys Acta* **1659**, 153–159.
38 Kořený L, Lukeš J & Oborník M (2010) Evolution of the haem synthetic pathway in kinetoplastid flagellates: an essential pathway that is not essential after all? *Int J Parasitol* **40**, 149–156.
39 Buchensky C, Almirón P, Mantilla BS, Silber AM & Cricco JA (2010) The *Trypanosoma cruzi* proteins TcCox10 and TcCox15 catalyze the formation of heme A in the yeast *Saccharomyces cerevisiae*. *FEMS Microbiol Lett* **312**, 133–141.
40 Changmai P, Horáková E, Long S, Černotíková-Stříbrná E, McDonald LM, Bontempi EJ & Lukeš J (2013) Both human ferredoxins equally efficiently rescue ferredoxin deficiency in *Trypanosoma brucei*. *Mol Microbiol* **89**, 135–151.
41 Panigrahi AK, Ogata Y, Zíková A, Anupama A, Dalley RA, Acestor N, Myler PJ & Stuart KD (2009) A comprehensive analysis of *Trypanosoma brucei* mitochondrial proteome. *Proteomics* **9**, 434–450.
42 Devaux S, Kelly S, Lecordier L, Wickstead B, Perez-Morga D, Pays E, Vanhamme L & Gull K (2007) Diversification of function by different isoforms of conventionally shared RNA polymerase subunits. *Mol Biol Cell* **18**, 1293–1301.
43 Basu S, Leonard JC, Desai N, Mavridou DAI, Tang KH, Goddard AD, Ginger ML, Lukeš J & Allen JWA (2013) Divergence of Erv1-associated mitochondrial import and export pathways in trypanosomes and anaerobic protists. *Eukaryot Cell* **12**, 343–355.
44 Saas J, Ziegelbauer K, Von Haeseler A, Fast B & Boshart M (2000) A developmentally regulated aconitase related to iron-regulatory protein-1 is localized in the cytoplasm and in the mitochondrion of *Trypanosoma brucei*. *J Biol Chem* **275**, 2745–2755.
45 Coustou V, Biran M, Besteiro S, Rivière L, Baltz T, Franconi JM & Bringaud F (2006) Fumarate is an essential intermediary metabolite produced by the procyclic *Trypanosoma brucei*. *J Biol Chem* **281**, 26832–26846.
46 Nakai Y, Nakai M, Lill R, Suzuki T & Hayashi H (2007) Thio modification of yeast cytosolic tRNA is an iron-sulfur protein-dependent pathway. *Mol Cell Biol* **27**, 2841–2847.
47 Fernández-Vázquez J, Vargas-Pérez I, Sansó M, Buhne K, Carmona M, Paulo E, Hermand D, Rodríguez-Gabriel M, Ayté J, Leidel S *et al*. (2013) Modification of $tRNA^{LYS}_{UUU}$ by elongator is essential for efficient translation of stress mRNAs. *PLoS Genet* **9**, e1003647.
48 Yamamoto M, Arimura H, Fukushige T, Minami K, Nishizawa Y, Tanimoto A, Kanekura T, Nakagawa M, Akiyama S-I & Furukawa T (2014) Abcb10 role in heme biosynthesis *in vivo*: Abcb10 knockout in mice causes anemia with protoporphyrin IX and iron accumulation. *Mol Cell Biol* **34**, 1077–1084.
49 Haynes CM, Yang Y, Blais SP, Neubert TA & Ron D (2010) The matrix peptide exporter HAF-1 signals a mitochondrial UPR by activating the transcription factor ZC376.7 in *C. elegans*. *Mol Cell* **37**, 529–540.
50 Vanhollebeke B, De Muylder G, Nielsen MJ, Pays A, Tebabi P, Dieu M, Raes M, Moestrup SK & Pays E (2008) A haptoglobin-hemoglobin receptor conveys innate immunity to *Trypanosoma brucei* in humans. *Science* **320**, 677–681.
51 Eckers E, Petrungaro C, Gross D, Riemer J, Hell K & Deponte M (2013) Divergent molecular evolution of the mitochondrial sulfhydryl: cytochrome *c* oxidoreductase Erv in opisthokonts and parasitic protists. *J Biol Chem* **288**, 2676–2688.
52 Kushnir S, Babiychuk E, Storozhenko S, Davey MW, Papenbrock J, De Rycke R, Engler G, Stephan UW, Lange H, Kispal G *et al*. (2001) A mutation of the mitochondrial ABC transporter Sta1 leads to dwarfism and chlorosis in the *Arabidopsis* mutant starik. *Plant Cell* **13**, 89–100.

53 Hyde BB, Liesa M, Elorza AA, Qiu W, Haigh SE, Richey L, Mikkola HK, Schlaeger TM & Shirihai OS (2012) The mitochondrial transporter ABC-me (ABCB10), a downstream target of GATA-1, is essential for erythropoiesis *in vivo*. *Cell Death Differ* **19**, 1117–1126.
54 Kořený L, Sobotka R, Kovářová J, Gnipová A, Flegontov P, Horváth A, Oborník M, Ayala FJ & Lukeš J (2012) Aerobic kinetoplastid flagellate *Phytomonas* does not require heme for viability. *Proc Natl Acad Sci USA* **109**, 3808–3813.
55 Lill R & Mühlenhoff U (2008) Maturation of iron-sulfur proteins in eukaryotes: mechanisms, connected processes, and diseases. *Annu Rev Biochem* **77**, 669–700.
56 Wohlgamuth-Benedum JM, Rubio MAT, Paris Z, Long S, Poliak P, Lukeš J & Alfonzo JD (2009) Thiolation controls cytoplasmic tRNA stability and acts as a negative determinant for tRNA editing in mitochondria. *J Biol Chem* **284**, 23947–23953.
57 Ginsburg H, Famin O, Zhang J & Krugliak M (1998) Inhibition of glutathione- dependent degradation of heme by chloroquine and amodiaquine as a possible basis for their antimalarial mode of action. *Biochem Pharmacol* **56**, 1305–1313.
58 Krauth-Siegel RL, Meiering SK & Schmidt H (2003) The parasite-specific trypanothione metabolism of trypanosoma and leishmania. *Biol Chem* **384**, 539–549.
59 Smith K, Opperdoes FR & Fairlamb AH (1991) Subcellular distribution of trypanothione reductase in bloodstream and procyclic forms of *Trypanosoma brucei*. *Mol Biochem Parasitol* **48**, 109–112.
60 Katoh K, Misawa K, Kuma K & Miyata T (2002) MAFFT: a novel method for rapid multiple sequence alignment based on fast Fourier transform. *Nucleic Acids Res* **30**, 3059–3066.
61 Gouy M, Guindon S & Gascuel O (2010) SeaView version 4: a multiplatform graphical user interface for sequence alignment and phylogenetic tree building. *Mol Biol Evol* **27**, 221–224.
62 Stamatakis A (2014) RAxML version 8: a tool for phylogenetic analysis and post-analysis of large phylogenies. *Bioinformatics* **30**, 1312–1313.
63 Vondrušková E, Van Den Burg J, Zíková A, Ernst NL, Stuart K, Benne R & Lukeš J (2005) RNA interference analyses suggest a transcript-specific regulatory role for mitochondrial RNA-binding proteins MRP1 and MRP2 in RNA editing and other RNA processing in *Trypanosoma brucei*. *J Biol Chem* **280**, 2429–2438.
64 Hashimi H, Zíková A, Panigrahi AK, Stuart KD & Lukeš J (2008) TbRGG1, a component of a novel multi-protein komplex involved in kinetoplastid RNA editing. *RNA* **14**, 970–980.
65 Carnes J, Trotter JR, Ernst NL, Steinberg A & Stuart K (2005) An essential RNase III insertion editing endonuclease in *Trypanosoma brucei*. *Proc Natl Acad Sci USA* **102**, 16614–16619.
66 Pfaffl MW (2001) A new mathematical model for relative quantification in real-time RT-PCR. *Nucleic Acids Res* **29**, e45.
67 Smíd O, Horáková E, Vilímová V, Hrdy I, Cammack R, Horváth A, Lukeš J & Tachezy J (2006) Knock-downs of iron-sulfur cluster assembly proteins IscS and IscU down-regulate the active mitochondrion of procyclic *Trypanosoma brucei*. *J Biol Chem* **281**, 28679–28686.
68 Hashimi H, Benkovičová V, Čermáková P, Lai DH, Horváth A & Lukeš J (2010) The assembly of F1FO-ATP synthase is disrupted upon interference of RNA editing in *Trypanosoma brucei*. *Int J Parasitol* **40**, 45–54.
69 Bechet J, Grenson M & Wiame J (1970) Mutations affecting the repressibility of arginine biosynthetic enzymes in *Sacchromyces cerevisiae*. *Eur J Biochem* **12**, 31–39.
70 Jacobs P, Jauniaux JC & Grenson M (1980) A cis-dominant regulatory mutation linked to the argB-argC gene cluster in *Saccharomyces cerevisiae*. *J Mol Biol* **139**, 691–704.
71 Amberg DC, Burke DJ & Strathern JN (2005) Methods in Yeast Genetics: A Cold Spring Harbor Laboratory Course Manual, pp. 59–76. Cold Spring Harbor Laboratory Press, Cold Spring Harbor, NY.
72 Güldener U, Heck S, Fiedler T, Beinhauer J & Hegemann JH (1996) A new efficient gene disruption cassette for repeated use in budding yeast. *Nucleic Acids Res* **24**, 2519–2524.
73 Igloi GL (1988) Interaction of tRNAs and of phosphorothioate-substituted nucleic acids with an organomercurial. Probing the chemical environment of thiolated residues by affinity electrophoresis. *Biochemistry* **27**, 3842–3849.